The 2012 World Congress on
Advances in Civil, Environmental, and Materials Research (ACEM' 12)
Seoul, Korea, August 26-30, 2012

Induced Modifications in the Structural, Electrical and Magnetic Properties of Sr-doped $BiFeO_3$ Multiferroics

Tanvir Hussain[1)], Saadat A. Siddiqi[1,2)], Shahid Atiq[1,3),*], Saira Riaz[1)] and Shahzad Naseem[1)]

[1]*Centre of Excellence in Solid State Physics, University of the Punjab, Lahore-54590, Pakistan*

[2]*Interdisciplinary Research Centre in Biomedical Materials (IRCBM), COMSATS Institute of Information Technology, Defense Road, Off Raiwind Road, Lahore, Pakistan*

[3)]Email: shahidatiqpasrur@yahoo.com

ABSTRACT

$BiFeO_3$ and the Sr doped $BiFeO_3$ samples were prepared by sol -gel auto-combustion technique using glycine as fuel. The powder was investigated with different characterization techniques to explore the properties of Sr doped $BiFeO_3$. X-ray diffraction (XRD) results confirmed the formation of pure $BiFeO_3$ peroskite type rhombohedral structure was found. XRD analysis also showed the presence of secondary phase of bismuth iron oxide ($Bi_2Fe_4O_9$) in all Sr-doped samples. The grain size was calculated from XRD results by using Scherrer formula and it was 11.062 nm. No considerable change in grain size was observed with varying amount of Sr doping. Frequency dependent dielectric measurements were performed at room temperature for all the samples $Bi_{1-x}Sr_xFeO_3$ (x = 0.00, 0.05, 0.10, 0.20, 0.30) from 100 Hz to 1 MHz. Magnetic properties were measured using vibrating sample magnetometer (VSM) which showed an enhancement in magnetization with increasing the concentrations of Sr. No remnant magnetization is present in pure $BiFeO_3$ material.

1. INTRODUCTION

Multifunctional materials have been vigorously investigated due to their application relevance and exciting fundamental physical properties. Concerning their technological applications, spintronic devices are nowadays most prominently used as hard disk drive read heads (Baibich 1988, Binasch 1989). Conventionally, magnetization is controlled by external magnetic fields. However, the implementation of magnetic fields of sufficient strength to switch the magnetization is technologically difficult on sufficiently small length scales. Hence, other approaches to control the magnetization are needed. From a technological point of view, electric fields are easy to implement on even very small length scales, power efficient and fully switchable. The ability to reversibly switch the magnetization orientation by an electric field is thus considered a milestone on the way to new functional spintronic devices. In this context, multiferroic materials are an important topic of current research, as multiferroic devices may be employed in future random access memories that combine the advantages of magnetic and ferroelectric random access memories (Scott 2007, Gajek 2007). Mostly multiferroic materials are divided in two major categories, type-I and type-II multiferroics (Khomskii 2009). In type-I multiferroics, the origin of magnetism and ferroelectricity are in different material and unfortunately the coupling of magnetic and ferroelectric subsystems in perovskites is

rather weak. In type-II multiferroics, electromagnetic coupling is very strong and ferroelectricity is induced due to certain ordering of magnetic moments only in magnetic state. In type-I multiferroics, most of the materials have perovskite structure ABO_3. In these materials ferroelectricity is generated due to transition metal "A" with d^o configuration whereas magnetism is produced by transition metal "B" with d^n (n is the odd number of electrons) configuration. $BiFeO_3$ is a type-I multiferroic material having rhombohedral perovskite structure. It has G-type antiferromagnetic structure in which each Fe^{3+} magnetic moment is surrounded by six Fe^{3+} nearest neighbours with antiparallel moments (Naik 2009). G-type structure is a spiral arrangement of the magnetic moments of Fe^{3+} ions, and the canted spins arising from Dzyloshinsii-Moriya (DM) interaction cause slight deviation from ideal antiferromagnetic behavior giving rise to weak ferromagnetism in $BiFeO_3$. Net magnetization of pure $BiFeO_3$ material is almost zero at room temperature (Ravindran 2006, Liu 2006, Neaton 2005). In this work, a sol-gel auto-combustion method was employed to synthesize Sr doped bismuth ferrite with composition of $Bi_{1-x}Sr_xFeO_3$ (x = 0.0, 0.05, 0.10, 0.20, 0.30). The structural, electric and magnetic properties of all the samples were investigated (Kim 2005, Bhushan 2010).

2. EXPERIMENTAL PROCEDURES

Sr-doped bismuth ferrite ($Bi_{1-x}Sr_xFeO_3$, x=0.0, 0.05, 0.10, 0.20, and 0.30) samples were prepared by sol-gel auto-combustion method by using glycine as a fuel agent. Bismuth nitrate penatahydrate [$Bi(NO_3)_3.5H_2O$, 99%, Sigma Aldrich], iron nitrate nanohydrate [$Fe(NO_3)_3.9H_2O$, 99.9%, Merck], strontium nitrate [$Sr(NO_3)_2$, 99.9%, Merck] and nitric acid (HNO_3) were used without further purification. $Bi(NO_3)_3.5H_2O$ is insoluble in distilled water, therefore, it is dissolved in 50 ml HNO_3 having Morality 3M. The salts of iron and strontium are dissolved in 50 ml distilled water (Singh 2010, Moure 2011). Both the solutions were mixed and appropriate quantity of glycine is added into solution. The mixture is placed on hot plate at 80 °C and continuously stirred using a magnetic capsule till it becomes a dark viscous resin. When the gel is formed, the temperature is increased up to 400 °C and continuous heating leads to auto-ignition of dried resin with the evolution of large quantity of gases. The brownish color ash obtained after combustion was analyzed for perovskite type $BiFeO_3$ Phase (Farhadi 2009). The fine powder was calcinated at 600 ºC temperature in furnace and pellets were formed in a steel dye of 16 mm diameter using the Apex hydraulic press. These pellets were sintered in air at 300 °C for 2h in a muffle furnace. The prepared samples of $Bi_{1-x}Sr_xFeO_3$ (x = 0.0, 0.05, 0.10, 0.20, 0.30) were characterized by using a Rigaku D/MAX-II A diffractometer with CuK_α radiations for phase and structural analysis. Dielectric properties were determined by using 1920 LCR meter to check storage ability of materials. A 7407-Lakeshore vibrating sample magnetometer (VSM) was used to obtain the hysteresis loops for the magnetic studies of samples.

3. RESULTS AND DISCUSSION

The X-ray diffraction patterns of all the samples, $Bi_{1-x}Sr_xFeO_3$ for x =0, 0.05, 0.10, 0.20 and 0.30 are shown in Fig. 1. All these patterns were obtained by varying 2θ from 0° to 80° having a step width of 0.02. The formation of pure $BiFeO_3$ is evident from the patterns with some impurity peaks of Bi_2O_3 and one unknown peak. The impurity peak of Bi_2O_3 is marked with (⁎) and unknown peak is marked with (●). As the concentration of Sr ions are increased, some peaks of secondary phase of $Bi_2Fe_4O_9$ appear and the intensity height of these peaks increases as the concentration of Sr ions is increased and it is also observed that the intensity peaks of impurity Bi_2O_3 and unknown impurity decrease as the

concentration of Sr ions is increased. The peaks of the secondary phase of bismuth iron oxide ($Bi_2Fe_3O_9$) is marked with (◇) as shown in Fig. 1(Wang 2009).

The crystallite size of the samples has been obtained by considering the most intense diffraction peaks of all the samples by using the Sherrer's formula (Khomchenko 2009).

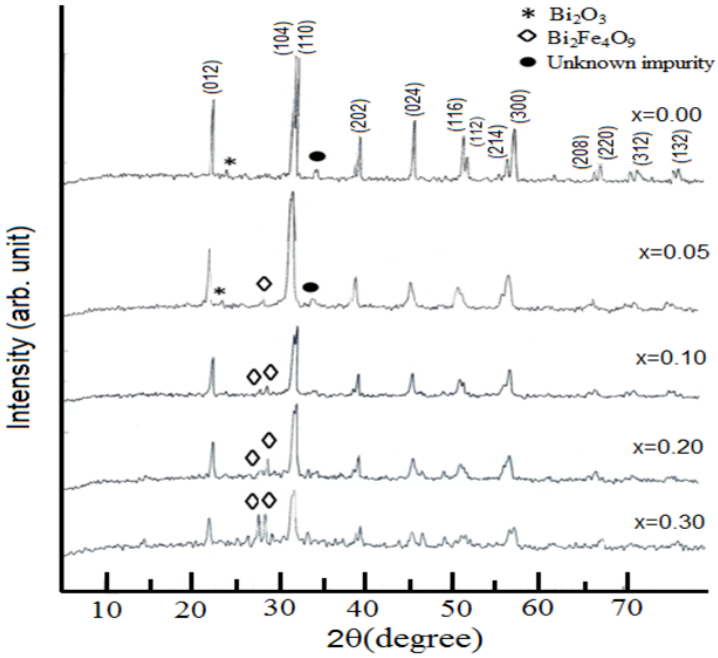

Fig. 1 XRD pattern of all the samples $Bi_{1-x}Sr_xFeO_3$ (x=0.0, 0.0.5, 0.10, 0.20, 0.30). The peak of Bi_2O_3 was marked by (∗) and unknown impurity peak was marked by (•). The peaks of secondary phase of bismuth iron oxide (Bi_2Fe4O_9) were marked by (◇).

The overall width of the most intense peaks of all samples remains the same. So the crystallite size of all samples $Bi_{1-x}Sr_xFeO_3$ remains almost same as shown in Fig. 2. The lattice parameters of unit cell were found out by using "CELL" software by putting the 2θ values of all diffraction peaks and then volume of each unit cell of all samples was found evaluated, as listed in Table 1. These values are in good agreement with values that has already been reported (Khomchenko 2009, Bhushan 2010).

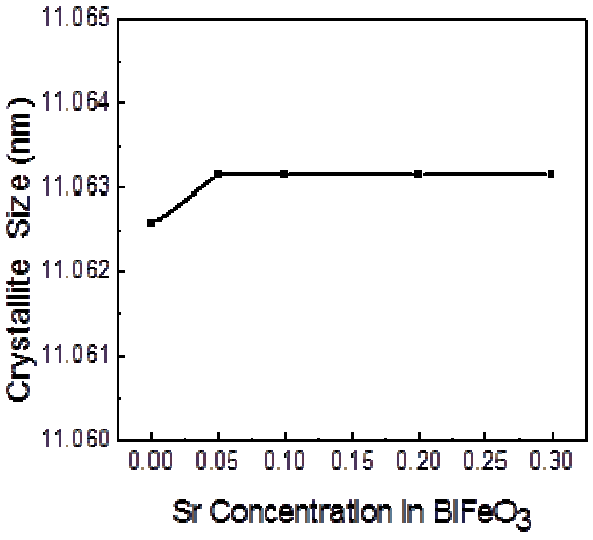

Fig. 2 Crystallite size vs. Sr concentration of in $Bi_{1-x}Sr_xFeO_3$ (x = 0.0, 0.05, 0.10, 0.20, 0.30).

Table 1 shows that a very small doping of Sr ion in $Bi_{1-x}Sr_xFeO_3$ (x = 0.05) decreases the unit cell volume, which is expected due to the appearance of oxygen vacancies and/or Fe^{4+} ions in the lattice. As the concentration of Sr ion increases from x = 0.05, both the lattice parameters "*a*" and "*c*" increase gradually. The increment in unit cell volume for all samples (x = 0.10, 0.20, 0.30,) is due to the large ionic radii of Sr^{+2} (1.18 Å) as compared to Bi^{+3} (1.03 Å) (Bhushan 2010, Palewicz 2010, Shannigrahi 2007).

Table 1 Calculated parameters and volume of all samples $Bi_{1-x}Sr_xFeO_3$

Stoichiometry	*a* (Å)	*c* (Å)	V(Å^3)
$BiFeO_3$	5.583272	13.86846	374.400519
$Bi_{0.9}Sr_{0.05}FeO_3$	5.583959	13.77611	371.998917
$Bi_{0.90}Sr_{0.1}0FeO_3$	5.585641	13.78502	372.463801
$Bi_{0.80}Sr_{0.20}FeO_3$	5.590091	13.80143	373.501607
$Bi_{0.70}Sr_{0.30}FeO_3$	5.595896	13.80447	374.360172

Dielectric constant (ε') and dielectric loss factor (ε'') measurements of samples $Bi_{1-x}Sr_xFeO_3$ (x = 0, 0.05, 0.10, 0.20 and 0.30) were taken at room temperature (25 °C) and samples were used in disk form with approximate diameter of 16 mm and thickness of all the samples in range of 1.2 to 1.5 mm. The dielectric constant and dielectric loss factor measurements of samples were evaluated by using the following equation [Shukla 2009].

$$\varepsilon' = \frac{t \times C_p}{A \times \varepsilon} = \frac{t \times C_p}{\pi(\frac{d}{2})^2 \times \varepsilon} \qquad (1)$$

Here, *t* is the thickness of pellet, C_p is the equivalent parallel capacitance obtained experimentally, ε is the permittivity of free space and *d* is the diameter of the electrodes. The dielectric loss is obtained from the measured vale of dissipation factor. Here dissipation factor and equivalent parallel capacitance is obtained directly from the measurements (Shukla 2009).

The dielectric constant of all samples has been measured in the frequency range 100 Hz to 1M Hz at room temperature. It is observed that dielectric constant is decreased rapidly by increasing frequency and dielectric constant becomes independent at high frequencies. The decrement in dielectric constant is considered due to the dielectric relaxation. The dielectric dispersion can be explained by Koop's theory. According to this theory the dielectric structure was imagined to be consisting on double layer, one layer is conducting and other layer is insulating. According to structural point of view, dielectric relaxation is directly related to orientational polarization (Liu, Kim 2005, Bhushan 2010, Shukla 2009, Moure 2011). When we apply external electric field then atoms of the dielectric material takes some time to align them in the direction of electric field and that

time is called relaxation time which is mostly equal to 10^{-9} s (Unruan 2012, Song 2012). It is observed that the decrement in dielectric constant with increasing frequency is assigned to the fact that atoms in the dielectric material need a finite time to align up their axis in the applied electric field direction (Unruan 2012). As the frequency of the electric field increases, a point is reached when charge carriers of dielectric do not align with applied electric field so polarization cannot reach at its saturation point and do not follow the alteration of electric field so the dielectric constant is decreased. when frequency of the field continuous to increase, at last, the polarization will hardly have started to move before the field reverses and makes no contribution to polarization and so dielectric constant becomes independent at very high frequencies. Another very important point of the decrement in dielectric constant is also related with the hopping of electrons from Fe^{2+} to Fe^{3+} ions and these electrons require large amount of energy (Song 2012). At low frequency, electric field does not provide enough energy to electron for hopping but as we increase the frequency of electric field then it provides more energy and at last a point is reached when hopping of electrons is started from Fe^{2+} to Fe^{3+}. Resultantly, the conductivity of the dielectric increases as frequency is increased and decrement is occurred in dielectric constant. The frequency-dielectric constant relationship of all the samples, $Bi_{1-x}Sr_xFeO_3$ (x = 0.0, 0.05, 0.10, 0.20, 0.30) is shown in Fig. 3.

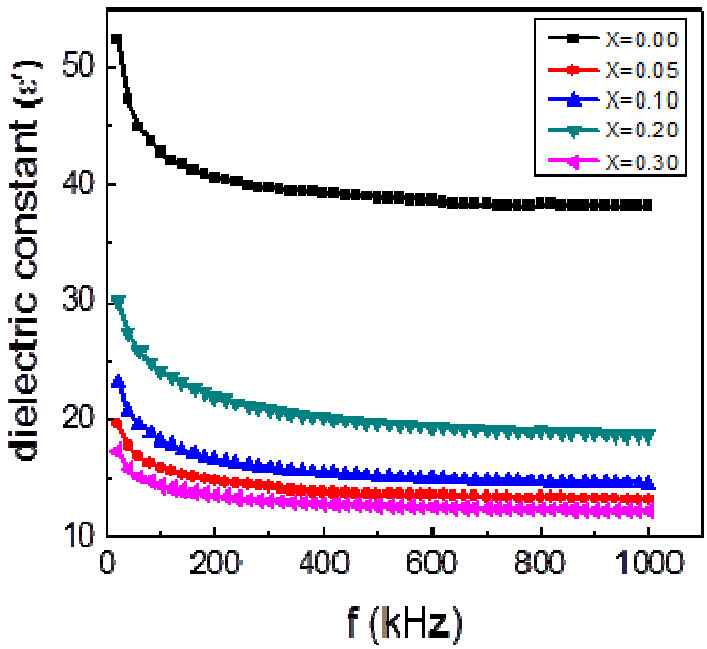

Fig. 3 Dependence of dielectric constant on frequency of all samples $Bi_{1-x}Sr_xFeO_3$ (x = 0.0, 0.05, 0.10, 0.20, 0.30).

As can be seen in the figure, the concentration of Sr ions increases in $BiFeO_3$, dielectric constant decreases to a very large extent because with Sr doping the conductivity of compound $BiFeO_3$ is increased (Jun 2005) and decrement occurs in dielectric constant. When the relaxation time of dielectric material and the frequency of the applied field become similar, a phase lag occurs. The energy absorbed in the dielectric material is called dielectric loss, which can be calculated by a relation:

$$\mathrm{Tan}\delta = \frac{\varepsilon''}{\varepsilon'} \qquad (2)$$

where, ε′ is the dielectric constant and ε″ is the dielectric loss of the material. The behavior of dielectric loss is similar to the dielectric constant. The dielectric loss of all compositions $Bi_{1-x}Sr_xFeO_3$ (x = 0.0, 0.05, 0.10, 0.20, 0.30) decrease with increasing frequency. The dielectric loss means loss of energy in dielectric material (Moure 2011, Shukla 2009). The dielectric loss of all the samples is shown in Fig. 4.

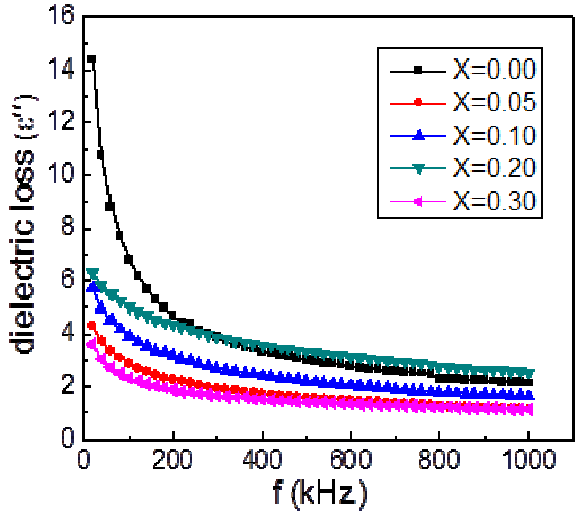

Fig. 4 Dependence of dielectric loss (ε″) on frequency of all the samples $Bi_{1-x}Sr_xFeO_3$ (x = 0.0, 0.05, 0.10, 0.20, 0.30)

Fig. 5 shows the magnetic hysteresis (M-H) loops of the samples. The M-H loops show that the saturation magnetization (M_s) of all the samples is achieved below 1000 Oe. It is clear from the loop of pure $BiFeO_3$, that the magnetization increases linearly with applied magnetic field and no spontaneous magnetization is observed. In addition, the value of remnant magnetization (M_r) was observed to be zero, depicting anti-ferromagnetic nature of $BiFeO_3$ (Ravindran 2006, Liu 2006). By doping of divalent Sr^{2+} ions in place of trivalent Bi^{3+} sites there is also a possibility of the presence of some oxygen vacancies in order to compensate the charge of $Bi_{1-x}Sr_xFeO_3$ material. It has been reported that the Mössbauer spectroscopy of Sr doped $BiFeO_3$ material shows no formation of Fe^{4+} or Fe^{2+} ions in $Bi_{1-x}Sr_xFeO_3$ material. Therefore it is indicated that oxygen vacancies must have been created in material to compensate the charge imbalance which is created by doping of Sr^{2+} ions in place of Bi^{3+} ions. In pure $BiFeO_3$, Fe^{3+}-O-Fe^{3+} chains show antiferromagnetic behavior (Bhushan 2011). By Sr^{2+} doping, oxygen vacancies are generated in material. Due to these vacancies the bond angle of Fe^{3+}-O-Fe^{3+} increases and the spin of Fe^{3+} ions are canted and net magnetization is induced. The value of magnetization increases with increasing doping concentration of Sr^{2+} ions because by doping Sr^{2+}, more oxygen vacancies are created and the bond angle of Fe^{3+}-O-Fe^{3+} continues to increase. Hence, more spins are canted and an enhancement occurs in magnetization [Wang 2009]. Oxygen vacancies are not the only factor to enhance the net magnetization of $Bi_{1-x}Sr_xFeO_3$ (x = 0.0, 0.05, 0.10, 0.20, 0.30). Ionic radii of the doped element also play an important role to enhance the magnetization of $BiFeO_3$ (Yang 2010, Jun 2005). The ionic radii of

doped element must be greater than that of Bi^{3+}. Owing to the greater ionic radii of the doped element, spiral spin structure is suppressed and the inversion symmetry is broken. This results in a change of structure into cycloidal type structure and net magnetization is induced in doped $BiFeO_3$ material. It is evident in Fig. 5 that the magnetization increases linearly by applying magnetic field and no M_r is present in pure $BiFeO_3$ material (Kim 2012, Xuelian 2009). After doping Sr^{2+} ions in $BiFeO_3$, its magnetization increases and maximum magnetization and coercivity (H_c) is achieved when the concentration of Sr^{2+} is x = 0.30. The values of M_s, M_r and H_c for this composition have been evaluated as, 0.867 emu/g, 0.175 emu/g and 366.64 Oe, respectively.

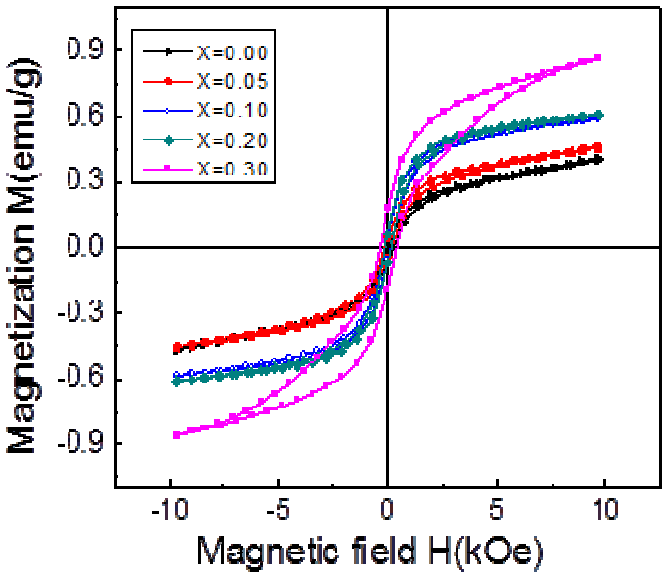

Fig. 5 M-H loops of $Bi_{1-x}Sr_xFeO_3$ (x = 0.00, 0.05, 0.10, 0.20, 0.30) samples

4. CONCLUSIONS

Pure phase $BiFeO_3$ was successfully synthesized by sol-gel auto-combustion technique. A dilute impurity phase of $Bi_2Fe_4O_9$ was detected in all Sr doped samples. Lattice parameters were changed with the substitution of Sr at the Bi sites. For x = 0 the estimated crystallite size was 11.062 nm and very small increment was observed in crystallite size with Sr doping. The dielectric constant of pure $BiFeO_3$ was found as 52 at 100 Hz frequency. It decreases with increasing frequency and becomes constant at high frequency. The dielectric constant also decreases with increasing Sr concentration and is found as 52 at 100 Hz for x = 0 composition. It decreases to 17.4 at 100 Hz for x = 0.30 composition. Magnetization of all the samples was enhanced with the increase in Sr content. From the M-H loop of pure $BiFeO_3$, it is observed that no remnant magnetization is present and a very small value of coercivity is noted. As the concentration of Sr doping increases in $BiFeO_3$, both the saturation magnetization and coercive field increase and become M_s= 0.867 emu/g and H_c = 336.64 G, respectively, for x = 0.30.

Acknowledgements

The authors would like to thank Dr. Muhammad Sabieh Anwar for his help in dielectric measurements.

REFERENCES

Baibich, M.N., Broto, J.M., Fert, A., Van Dau, F.N., Petro, F., Eitenne, P., Creuzet, G., Friederich, A., and Chazelas, J. (1988), "Giant Magnetoresistance of (001) Fe / (001) Cr Magnetic Superlattices", *Phys. Rev. Lett*., **61**(21), 2472–2475.

Binasch, G., Graunberg, P., Saurenbach, F. and Zinn, W. (1989), "Enhanced magnetoresistance in layered magnetic structures with antiferromagnetic interlayer exchange", *Phys. Rev. B*, **39**(7), 4828–4830.

Bhushan, B., Basumallik, A., Vasanthacharya, N.Y., Kumar, S. and Das, D. (2010), "Sr induced modification of structural, optical and magnetic properties in $Bi_{1-x}Sr_xFeO_3$ (x = 0, 0.01, 0.03, 0.05 and 0.07) multiferroic nanoparticles", *Solid State Sci*., **12**(7), 1063-1069.

Dai, Z. and Akishige, Y. (2010), "Electrical properties of multiferroic $BiFeO_3$ ceramics synthesized by spark plasma sintering", *J. Phys. D: Appl. Phys*., **43**(44), 445403, 1-5.

Farhadi, S. and Zaidi, M. (2009), "Preparation and characterization of pure single-phase $BiFeO_3$ nanoparticles through thermal decomposition of the heteronuclear $Bi[Fe(CN)_6]\cdot 5H_2O$ complex", *J. Mol. Catal. A: Chem*., **299**(15), 2959–2965.

Gajek, M., Bibes, M., Fusil, S., Bouzehouane, K., Fontcuberta, J., Barthelemy, A. and Fert, A. (2007), "Tunnel junctions with multiferroic barriers", *Nature Mater*., **6**(1), 296 – 302.

Jun, Y.K., Moon, W.T., Chang, C.M., Kima, H.S., Ryu, H.S., Kim, J.W., Kim, K.H. and Hong, S. H. (2005), "Effects of Nb-doping on electric and magnetic properties in multi-ferroic $BiFeO_3$ ceramics", *Solid State Commun*., **135**(1-2), 133-137.

Kim, A.Y., Han, S.H., Kang, H.W., Lee, H.G., Kim, J.S. and Cheon, C.I. (2012), "Dielectric and magnetic properties of $BiFeO_3$ ceramics prepared by hydrothermal synthesis", *Ceram. Int*., **38**(1), S397-S401.

Kim, J.K., Kim, S.S. and Kim W.J. (2005), "Sol-gel synthesis and properties of multiferroic $BiFeO_3$", *Mater. Lett*., **59**(29-30), 4006-4009.

Khomchenko, V.A., Kiselev, D.A., Kopcewicz, M., Maglione, M., Shvartsman, V.V., Borisov, P., Kleemann, W., Lopes, A.M.L., Pogorelov, Y.G., Araujo, J.P.,

Khomskii, D. (2009), "Classifying multiferroics: Mechanisms and effects", Physics, **2**(1), 20-28.

Liu, H., Liu, Z., Liu, Q. and Yao, K. (2006), "Ferroelectric properties of $BiFeO_3$ films grown by sol–gel process", *Thin Solid Films*, **500**(1-2), 105-109.

Moure, A., Tartaj, J. and Moure, C. (2011), "Processing and characterization of Sr doped $BiFeO_3$ multiferroic materials by high energetic milling", *J. Alloys Compd*., **509**(25), 7042-7046.

Naik, V.B. and Mahendiran, R. (2009), "Magnetic and magnetoelectric studies in pure and cation doped $BiFeO_3$", *Solid State Commun*., **149**(19-20), 754-758.

Neaton, J.B., Ederer, C., Waghmare, U.V., Spaldin, N.A. and Rabe, K.M. (2005), "First-principles study of spontaneous polarization in multiferroic $BiFeO_3$", Phys. Rev. B, **71**(1), 014113, 1-8.

Palewicz, A., Sosnowska, I., Przeniosło, R. and Hewat, A.W. (2010), "$BiFeO_3$ Crystal Structure at Low Temperatures", (2010), *Proceedings of the 8th National Meeting of Synchrotron Radiation Users*, Podlesice, September.

Ravindran, P., Vidya, R., Kjekshus, A. and Fjellvag, H., (2006), “Theoretical investigation of magnetoelectric behavior in $BiFeO_3$”, *Phys. Rev. B*, **74**(22), 224412, 1-18.
Rubinger, R.M., Sobolev, N.A., Vieira, J.M. and Kholkin, A.L. (2009), “Doping strategies for increased performance in $BiFeO_3$”, *J. Magn. Magn. Mater.*, **321**(11), 1692-1698.
Scott, J.F. (2007), “Data storage: Multiferroic memories”, *Nature Mater*., **6**(1), 256 – 257.
Shannigrahi, S.R., Huang, A. and Chandrasekhar, N. (2007), “Sc modified multiferroic $BiFeO_3$ thin films prepared through a sol-gel process”, *Appl. Phys. Lett*., **90**(2), 022901, 1-3.
Shukla, R.K., Srivastava, A., Dubey, K.C. and Kumar, N. (2009), “Dielectric properties of zinc oxide pellets”, *International Conference on Emerging Trends in Electronic and Photonic Devices & Systems*, December.
Singh, P., Park, Y.A., Sung, K.D., Hur, N., Jung, J.H., Noh, W.S., Kim, J.Y.,Yoon, J. and Jo, Y. (2010), “Magnetic and ferroelectric properties of epitaxial Sr-doped thin films”, *Solid State Commun*., **150**(9-10), 431-434.
Song, G.L., Zhang, H.X., Wang, T.X., Yang, H.G. and Chang, F.G. (2012), “Effect of Sm, Co co-doping on the dielectric and magnetoelectric properties of $BiFeO_3$ polycrystalline ceramics”, *J. Magn. Magn. Mater*., **324**(13), 2121-2126.
Unruan, M., Sareein, T., Chandarak, S., Hunpratub, S., Thongbai, P., Maensiri, S. and Yimnirun, R. (2012), “Aging and stress-dependent dielectric properties of multiferroic bismuth ferrite ceramics”, *Mater. Lett*., **70**(1), 185-188.
Wang, L.Y., Wang, D.H., Huang, H.B., Han, Z.D., Cao, Q.Q., Gu, B.X. and Du, Y.W. (2009), “The magnetic properties of polycrystalline $Bi_{1-x}Sr_xFeO_3$ ceramics”, *J. Alloys Compd*., **469**(1-2), 1-3.
Xuelian, Y., Xiaoqiang A., (2009), “Enhanced magnetic and optical properties of pure and (Mn, Sr) doped $BiFeO_3$ nanocrystals”, *Solid State Commun*., **149** (17-18), 711-714.
Yang, C., Jiang, J.S., Qian, F.Z., Jiang, D.M. Wang, C.M. and Zhang, W.G. (2010), “Effect of Ba doping on magnetic and dielectric properties of nanocrystalline $BiFeO_3$ at room temperature”, *J. Alloys Compd*., **507**(1), 29-32.